

Anisotropic elastic properties and ideal uniaxial compressive strength of TiB_2 from first principles calculations

Sun Min(孙敏), Wang Chong-Yu(王崇愚), Liu Ji-Ping(刘吉平)

Citation: Chin. Phys. B . 2018, 27(7): 077103. **doi:** 10.1088/1674-1056/27/7/077103

Journal homepage: http://cpb.iphy.ac.cn; http://iopscience.iop.org/cpb

What follows is a list of articles you may be interested in

Electronic structures and optical properties of HfO_2-TiO_2 alloys studied by first-principles GGA+ *U* approach

Jin-Ping Li(李金平), Song-He Meng(孟松鹤), Cheng Yang(杨程), Han-Tao Lu(陆汉涛), Takami Tohyama(遠山貴巳)
Chin. Phys. B . 2018, 27(2): 027101. **doi:** 10.1088/1674-1056/27/2/027101

Optical properties of anatase and rutile TiO_2 studied by GGA+*U*

Jinping Li(李金平), Songhe Meng(孟松鹤), Liyuan Qin(秦丽媛), Hantao Lu(陆汉涛)
Chin. Phys. B . 2017, 26(8): 087101. **doi:** 10.1088/1674-1056/26/8/087101

Visible light absorption of (Fe, C/N) co-doped $NaTaO_3$: DFT+*U*

Peng-Li Tian(田鹏莉), Zhen-Yi Jiang(姜振益), Xiao-Dong Zhang(张小东), Bo Zhou(周波), Ya-Ru Dong(董亚茹), Rui Liu(刘睿)
Chin. Phys. B . 2017, 26(8): 087102. **doi:** 10.1088/1674-1056/26/8/087102

First-principle study of the structural, electronic, and optical properties of SiC nanowires

Wei-Hu Zhang(张威虎), Fu-Chun Zhang(张富春), Wei-Bin Zhang(张伟斌), Shao-Lin Zhang(张绍林), Woochul Yang
Chin. Phys. B . 2017, 26(5): 057103. **doi:** 10.1088/1674-1056/26/5/057103

Stability, electronic structures, and mechanical properties of Fe-Mn-Al system from first-principles calculations

Ya-Hui Liu(刘亚会), Xiao-Yu Chong(种晓宇), Ye-Hua Jiang(蒋业华), Jing Feng(冯晶)
Chin. Phys. B . 2017, 26(3): 037102. **doi:** 10.1088/1674-1056/26/3/037102

Anisotropic elastic properties and ideal uniaxial compressive strength of TiB_2 from first principles calculations

Min Sun(孙敏)[1], Chong-Yu Wang(王崇愚)[2,‡], and Ji-Ping Liu(刘吉平)[1,†]

[1] *School of Material Science and Engineering, Beijing Institute of Technology, Beijing* 100081, *China*
[2] *Department of Physics, Tsinghua University, Beijing* 100084, *China*

(Received 15 June 2018; published online 25 June 2018)

The structural, anisotropic elastic properties and the ideal compressive and tensile strengths of titanium diboride (TiB_2) were investigated using first-principles calculations based on density functional theory. The stress–strain relationships of TiB_2 under $\langle 10\bar{1}0\rangle$, $\langle \bar{1}2\bar{1}0\rangle$, and $\langle 0001\rangle$ compressive loads were calculated. Our results showed that the ideal uniaxial compressive strengths are $|\sigma_{\langle \bar{1}2\bar{1}0\rangle}| = 142.96$ GPa, $|\sigma_{\langle 0001\rangle}| = 188.75$ GPa, and $|\sigma_{\langle 10\bar{1}0\rangle}| = 245.33$ GPa, at strains -0.16, -0.32, and -0.24, respectively. The variational trend is just the opposite to that of the ideal tensile strength with $\sigma_{\langle 10\bar{1}0\rangle} = 44.13$ GPa, $\sigma_{\langle 0001\rangle} = 47.03$ GPa, and $\sigma_{\langle \bar{1}2\bar{1}0\rangle} = 56.09$ GPa, at strains 0.14, 0.28, and 0.22, respectively. Furthermore, it was found that TiB_2 is much stronger under compression than in tension. The ratios of the ideal compressive to tensile strengths are 5.56, 2.55, and 4.01 for crystallographic directions $\langle 10\bar{1}0\rangle$, $\langle \bar{1}2\bar{1}0\rangle$, and $\langle 0001\rangle$, respectively. The present results are in excellent agreement with the most recent experimental data and should be helpful to the understanding of the compressive property of TiB_2.

Keywords: ideal compressive strength, electronic structure, elastic property, first principles calculation

PACS: 71.15.MB, 71.15.–m, 81.05.Je, 62.20.–x **DOI:** 10.1088/1674-1056/27/7/077103

1. Introduction

TiB_2 is well known as a ceramic material with many unique physical properties, such as high hardness, elastic modulus, strength to weight ratio, wear resistance, good thermal and electrical conductivities.[1] The range of potential applications of TiB_2 is extensive, including nose tip and sharp leading edges of hypersonic vehicles, hot structure components for scramjet engines, impact resistant armor, cutting tools, wear resistant parts, grain refiner, as well as reinforcements in various composite materials such as special steel. In addition, the high electrical conductivity enables machining of titanium borides using the electrical discharge machining.[2,3] Thus, in the last two decades, TiB_2 has received increasing attention in its experimental and theoretical researches.

The physical and mechanical properties are important to the practical performance. Especially, profound insight of the ideal strength of TiB_2 is of great importance not only in deepening the understanding of intrinsic properties of TiB_2 but also in realistic structural applications. The ideal strength of a material is the minimum stress at which a perfect crystal begins to deform plastically, whereas the yield point is the point where nonlinear deformation begins.[4] The ideal strength of materials, which is dominated by the behavior of valence electrons and ions, represents an upper limit of the strength that real materials can have under a given load, and thus, has attracted great interest in material science.[5]

Based on the first principles approaches and the developments in super-computers, the ideal strength can now be investigated at the atomic level. The strength is commonly considered in terms of compressive strength, tensile strength, and shear strength with corresponding applied loads.[6,7] The atomistic deformation mechanisms and stress–strain relationships of tensile and shear deformations have been extensively examined for TiB_2. Zhou *et al.*[8] investigated the structural, stability, chemical bonding, hardness, and mechanical properties of 3d, 4d, 5d transition metal diboride TMB_2 using first principles calculations and pointed out that the number of valence electrons of the transition metals has strong effects on the above properties. The ideal shear and tensile strengths of ZrB_2, HfB_2, and TiB_2 were studied by Zhang *et al.*[9] using the first-principles calculations. Chen *et al.*[10] estimated the temperature-dependent ideal tensile strength of the AlB_2 like diborides. The anisotropic elastic and thermal expansions of the titanium borides were calculated by Sun *et al.*[3] using first-principles methods. Afaf Saai *et al.*[11] used a sequential multi-scale approach to evaluate the degradation of TiB_2 as a function of its microstructure.

Experimental works about the compressive strength of TiB_2 were also reported. Munro[12] measured the physical, mechanical, and thermal properties of polycrystalline TiB_2, and determined a consistent set of trend values of these properties on the dependence of density and grain size. At room temperature, Munro estimated that the dependence of the compressive strength on the density is approximately linear, rang-

†Corresponding author. E-mail: ilphysics@163.com
‡Corresponding author. E-mail: cywang@mail.tsinghua.edu.cn

© 2018 Chinese Physical Society and IOP Publishing Ltd

ing from 1.1 GPa at 3.8 g/cm to 1.8 GPa at 4.5 g/cm. The Hugoniot-measurements were performed on the TiB_2 polycrystal by Mashimo *et al.*[13] to investigate the elastoplastic transition using the inclined-mirror method combined with the powder gun and two-stage gas gun. The Hugoniot-elastic limit stress was measured to be approximately 12 GPa. These studies have deepened the understanding of the single crystals of TiB_2.

However, the calculation of the ideal compressive strength of TiB_2 is still an open question, and there is scant confirmed reports on this issue. In fact, the ideal compressive strength, like the ideal tensile and shear strength, is one of the primary intrinsic mechanical properties of a solid material and is fundamental for the development of practical applications.[7]

In the light of this background, in the present work, by performing the first-principles calculations based on density functional theory, the ideal uniaxial compressive strength of TiB_2 single crystal is studied. The organization of the paper is as follows. Section 2 introduces the methodology for calculating the theoretical strength under a uniaxial load. Section 3 presents and discusses the main results of this work. Finally, the conclusions are presented in Section 4. The results fill the void in the literature regarding the ideal compressive strength of TiB_2.

2. Calculational details

The first principles calculations were performed within the generalized-gradient approximation of Perdew–Burke–Ernzerhoff[14] for the exchange–correlation functional as implemented in the Vienna *abinitio* simulation package code.[15] The cut-off energy of atomic wave functions was set to be 415 eV in all calculations after the convergence test. A special k-point sampling method was utilized for the integration by setting $11\times11\times10$ for TiB_2 with Monkhorst–Pack scheme[16] in the first irreducible Brillouin zone. The break condition for the electronic self-consistency was set to be 10^{-5} eV. The ionic relaxation was stopped when the forces on all of the atoms were less than 0.02 eV/Å.

In order to investigate the anisotropic mechanical properties, the elastic stiffness and other mechanical properties were estimated. The crystal structure of TiB_2 considered in the current paper has the hexagonal symmetry with Ti atoms forming a metallic hexagonal structure and B atoms situated interstitially between the Ti-layers as is shown in Fig. 1. The elastic constants were estimated from first-principles strain-stress relationships as implemented by Milman *et al.*[17] Specifically, according to Hooke's law, the elastic constants can be defined by means of a Taylor expansion of the total energy $E(V,\{\varepsilon_i\})$ with respect to a small strain δ for the system[18]

$$E(V,\{\varepsilon_i\}) = E(V_0,0) + V_0\left(\sum_{i=1}^{6}\tau_i e_i + \frac{1}{2}\sum_{i=1}^{6}\sum_{j=1}^{6}C_{ij}e_i e_j + O(e^3)\right), \quad (1)$$

$$\Delta E = V_0\left(\sum_{i=1}^{6}\tau_i e_i + \frac{1}{2}\sum_{i=1}^{6}\sum_{j=1}^{6}C_{ij}e_i e_j + O(e^3)\right), \quad (2)$$

where C_{ij} are the elastic constants $C_{ij} = \frac{1}{V}\left[\frac{\partial^2 E(V,\varepsilon_k)}{\partial\varepsilon_i\partial\varepsilon_j}\right]_{\varepsilon=0}$ $(i,j,k=1,\ldots,6)$, V_0 is the unstrained volume of the unit cell, τ_i are related to the stress on the lattice $\tau_i = \frac{1}{V}\left[\frac{\partial E(V,\varepsilon_j)}{\partial\varepsilon_i}\right]_{\varepsilon=0}$ $(i,j=1,\ldots,6)$, and e_i are the components of the strain tensor ε,

$$\varepsilon = \boldsymbol{I}\cdot\boldsymbol{D} = \frac{1}{2}\begin{pmatrix} 2e_1 & e_6 & e_5 \\ e_6 & 2e_2 & e_4 \\ e_5 & e_4 & 2e_3 \end{pmatrix} \quad (3)$$

in conventional elastic theory notation and $\boldsymbol{I}$ represents the identity matrix. TiB_2 crystallizes in AlB_2-type structure with the space group $P6/mmm$ (No. 191) and therefore the number of independent elastic constants is reduced to 5, i.e., C_{11}, C_{12}, C_{13}, C_{33}, and C_{44},

$$\begin{pmatrix} C_{11} & C_{12} & C_{13} & 0 & 0 & 0 \\ C_{12} & C_{11} & C_{13} & 0 & 0 & 0 \\ C_{13} & C_{13} & C_{11} & 0 & 0 & 0 \\ 0 & 0 & 0 & C_{44} & 0 & 0 \\ 0 & 0 & 0 & 0 & C_{44} & 0 \\ 0 & 0 & 0 & 0 & 0 & (C_{11}-C_{12})/2 \end{pmatrix}. \quad (4)$$

The elastic constants can be obtained by applying an appropriate set of distortions with the distortion parameter δ as shown in Table 1.

Table 1. The five applied strain configurations used to calculate the five independent elastic constants of the hexagonal TiB_2 and the corresponding strain energy density–strain ($\Delta E/V_0 \sim \delta$) relation.

Strain configuration	Strain energy density–strain relation
$\boldsymbol{e} = (\delta,\delta,0,0,0,0)$	$\Delta E/V_0 = (C_{11}+C_{12})\delta^2$
$\boldsymbol{e} = (0,0,0,0,0,\delta)$	$\Delta E/V_0 = \frac{1}{4}(C_{11}-C_{12})\delta^2$
$\boldsymbol{e} = (0,0,\delta,0,0,0)$	$\Delta E/V_0 = \frac{1}{2}C_{33}\delta^2$
$\boldsymbol{e} = (0,0,0,\delta,\delta,0)$	$\Delta E/V_0 = C_{44}\delta^2$
$\boldsymbol{e} = (\delta,\delta,\delta,0,0,0)$	$\Delta E/V_0 = (C_{11}+C_{12}+2C_{13}+C_{33}/2)\delta^2$

For the purpose of analyzing the stress response to strain in the main crystal directions, an orthogonal unit cell having six atoms was used to calculate the ideal strength of TiB_2[9] as shown in Fig. 1(b). The axes orientations of the orthogonal unit cell are along the $\langle 10\bar{1}0\rangle$ (a axis), $\langle \bar{1}2\bar{1}0\rangle$ (b axis), and $\langle 0001\rangle$ (c axis) directions of the primitive cell. The calculation approaches of tensile strength and compressive strength are similar to those of previous studies.[19,20] The stress–strain curves were calculated by incrementally deforming the unit cell in the selected strain direction. The atomic basis vectors orthogonal to the applied strain were simultaneously relaxed until the other stress components disappeared. Meanwhile, all the internal freedoms of the atom were relaxed until the atoms reached their equilibrium at each step.

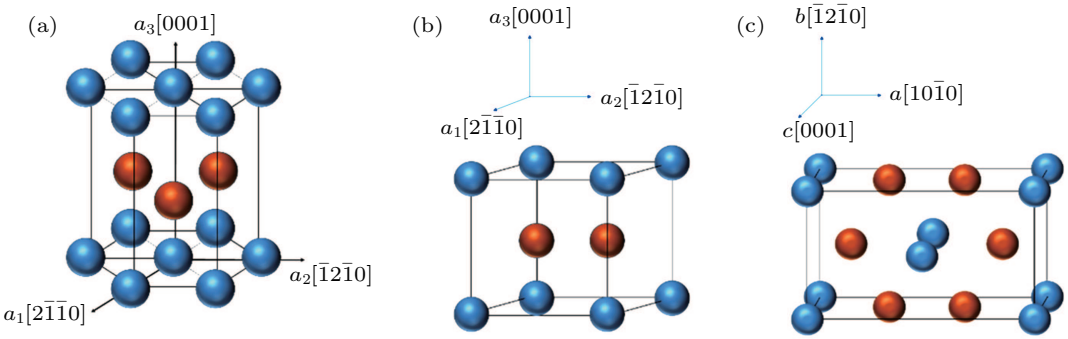


Fig. 1. Schematic illustrations of (a) the hexagonal crystal structure, (b) the primitive cell, and (c) the orthogonal unit cell of TiB_2. The blue and red atoms are Ti and B atoms, respectively.

3. Results and discussion

3.1. Equilibrium geometry of TiB_2

TiB_2 crystallizes in the hexagonal AlB_2 structure designated as $C32$ with the space group $P6/mmm$. There are three atoms in the unit cell, one Ti atom at the origin and two B atoms at (1/3, 2/3, 1/2) and (2/3, 1/3, 1/2), respectively. The optimized cell constants and the previously calculated and experimental values[2,21,22] are listed in Table 2. The lattice constants a and c are in excellent agreement with the available experimental and calculated results. The average deviation is less than 0.3%, which demonstrates the reliability of the present calculations.

Table 2. Calculated equilibrium lattice constants of TiB_2 compared with available experimental and theoretical data.

	a/Å	c/Å
This work	3.033	3.231
Ref. [20] (Exp.)	3.032	3.229
Ref. [21] (Exp.)	3.038	3.22
Ref. [2] (Cal.)	3.029	3.220

3.2. Elastic constants, polycrystalline moduli, and hardness

A hexagonal TiB_2 crystal has six different elastic constants (c_{11}, c_{12}, c_{13}, c_{33}, c_{44}, and c_{66}), but only five of them are independent since $c_{66} = (c_{11} - c_{12})/2$. The compliance constants $\{S\} = \{C^{-1}\}$ were also calculated by solving the inverse of the elastic constant matrix by using MATLAB. The calculated elastic and compliance constants of TiB_2 are shown in Table 3. Notably, the anisotropic parameters in elasticity, c_{33}/c_{11} and c_{44}/c_{66} are smaller than unity, which indicates that the atomic bonding along the a-axis is stronger than that along the c-axis. This is consistent with the picture that the crystal structure of TiB_2 is of the layered-type. Intra the B layer, the B atoms form a 2D graphite-like geometric structure by sharing the valence electrons through sp^2 hybridization. Each B atom establishes three σ-type sp^2–sp^2 bonds with its adjacent B atoms. The bonding in the Ti plane is mainly metallic. While the nature of the bonding inter the Ti and B sub-layers is the mixture of ionic–covalent interactions.[23] Thus, the B–B bond is stronger than the Ti–B bond, which could be the main reason for the anisotropic elasticity of the TiB_2 structure. The intrinsic mechanical stability of TiB_2 can be justified by the Born–Huang criterion. For a hexagonal structure, the criterion can be expressed as[24]

$$c_{44} > 0, \quad c_{11} > |c_{12}|, \quad (c_{11} + c_{12})c_{33} > 2c_{13}^2. \tag{5}$$

The elastic constants in Table 3 completely satisfy the above stability conditions.

Table 3. Calculated elastic constants and compliance constants of TiB_2 from the primitive cells. Availabel experimental and theoretical data are listed for comparison.

	c_{11}/GPa	c_{12} /GPa	c_{13} /GPa	c_{33}/GPa	c_{44}/GPa
This work	648	72	116	454	257
Ref. [25] (Exp.)	655	57	98	455	263
Ref. [3] (Cal.)	654	64.2	96.9	459	258.1
Ref. [26] (Cal.)	650	79	100	443	256
	s_{11}/GPa^{-1}	s_{12}/GPa^{-1}	s_{13}/GPa^{-1}	s_{33}/GPa^{-1}	s_{44}/GPa^{-1}
This work	0.0016248	0.0000295	0.0003867	0.0024003	299968

Based on the obtained elastic and compliance constants, the bulk modulus B and shear modulus G can be calculated according to the Voigt–Reuss–Hill method.[27] The Voigt approximation assumes a uniform strain throughout a crystalline material and has[28]

$$B_{\mathrm{V}} = \frac{1}{9}(c_{11} + c_{22} + c_{33}) + \frac{2}{9}(c_{12} + c_{23} + c_{13}), \tag{6}$$

$$G_{\mathrm{V}} = \frac{1}{15}(c_{11} + c_{22} + c_{33}) - \frac{1}{15}(c_{12} + c_{23} + c_{13}) + \frac{1}{5}(c_{44} + c_{55} + c_{66}). \tag{7}$$

The Reuss approximation is based on the assumption of a uniform stress applied on the crystalline material and has[29]

$$B_{\mathrm{R}} = \frac{1}{(s_{11} + s_{22} + s_{33}) + 2(s_{12} + s_{23} + s_{13})}, \tag{8}$$

$$G_{\mathrm{R}} = \frac{15}{4(s_{11} + s_{22} + s_{33}) - 4(s_{12} + s_{23} + s_{13}) + 3(s_{44} + s_{55} + s_{66})}, \tag{9}$$

where

$$c_{22} = c_{11}, \quad s_{22} = s_{11},$$
$$c_{23} = c_{13}, \quad s_{23} = s_{13},$$
$$c_{55} = c_{44}, \quad s_{55} = s_{44},$$
$$c_{66} = \frac{1}{2}(c_{11} - c_{12}), \quad s_{66} = 2(s_{11} - s_{12}). \tag{10}$$

The Voigt and Reuss approximations represent the upper and lower bounds of the real modulus. Using energy considerations, Hill recommended that a practical estimate of the bulk and shear moduli are the arithmetic means of the two extremes[30]

$$B_{\mathrm{H}} = \frac{1}{2}(B_{\mathrm{V}} + B_{\mathrm{R}}), \tag{11}$$
$$G_{\mathrm{H}} = \frac{1}{2}(G_{\mathrm{V}} + G_{\mathrm{R}}). \tag{12}$$

Furthermore, the Young's modulus E and Poisson ratio ν are obtained in the light of the following equations:

$$E = \frac{9B_{\mathrm{H}}G_{\mathrm{H}}}{3B_{\mathrm{H}} + G_{\mathrm{H}}}, \tag{13}$$
$$\nu = \frac{3B_{\mathrm{H}} - 2G_{\mathrm{H}}}{2(3B_{\mathrm{H}} + G_{\mathrm{H}})}. \tag{14}$$

It is well acknowledged that hardness can be utilized as an indication of machinability of ceramics. Chen *et al.*[31] has given a theoretical definition for the Vicker's hardness, which is correlated to shear modulus G and can be estimated by the following formula:

$$H_{\mathrm{V}} = 0.151G. \tag{15}$$

Table 4. The bulk modulus (GPa), shear modulus (GPa), Young's modulus (GPa), Poisson's ratio and Vicker's hardness (GPa) for TiB_2 by means of Voigt–Reuss–Hill approximation.

	B_{V}	B_{R}	G_{V}	G_{R}	B_{H}	G_{H}	E	ν	H_{V}
This work	262.00	257.70	256.80	250.41	259.85	253.61	574.06	0.13	38.30
Ref. [3] (Cal.)	253.7	249	262.8	257.4	251.4	260.1	630.5	0.069	39.3
Ref. [32] (Cal.)	256.4	252	262.3	257	254.2	260	586.9	0.12	
Ref. [33] (Exp.)					253	259			35
Ref. [25] (Exp.)					250.0	262.6	583.5	0.111	
Ref. [12] (Exp.)					240	255	565	0.11	

The calculated bulk modulus, shear modulus, Young's modulus, Poisson ratio, and hardness are listed in Table 4. The calculated results in Table 4 show a good agreement with the reported theoretical and experimental data.[3,12,25,32,33] Bulk modulus B reflects the resistance to volume change, shear modulus G reflects the resistance to shape change, and the Young's modulus E describes the material's strain response to uniaxial stress in the direction of the stress.[8] The relatively high values of B, G, and E of TiB_2 make it possess many superior mechanical properties. According to Pugh's empirical rule,[34] the ductile/brittle behaviors of a material are closely related to the ratio of G/B. It is considered that the ductile behavior is associated with $G/B < 0.5$ and $G/B > 0.5$ means brittleness. For TiB_2, the calculated results evidently indicate that G/B is larger than 0.5, implying its brittle nature. The small value of Possion's ratio 0.13 indicates the strong covalence in TiB_2. The calculated hardness is 38.2 GPa, which is a bit larger than the reported experimental datum 35 GPa.[33]

3.3. Theoretical tensile and compressive strength of TiB_2

Figures 2(a)–2(f) show the relationships of energy and stress with the applied strain for TiB_2 that is pulled in $\langle 10\bar{1}\rangle$, $\langle \bar{1}2\bar{1}0\rangle$, and $\langle 0001\rangle$ directions respectively with full relaxations along the perpendicular axes.

It is seen from Figs. 2(a), 2(c), and 2(e) that the total energy profiles have a parabolic, convex character. With increasing elongations, the curves reach their inflexion points ($\frac{\mathrm{d}^2E}{\mathrm{d}\varepsilon^2} = 0$, where E is the total energy and ε is the corresponding deformed strain) and become concave. The inflexion points for $[10\bar{1}0]$, $[\bar{1}2\bar{1}0]$, and $[0001]$ uniaxial loadings occur at $\varepsilon = 0.16, 0.26, 0.36$ for tension and $\varepsilon = -0.22, -0.16, -0.30$ for compression.

For uniaxial compressive deformation, the stress τ is given by $\tau = \frac{1}{V(\varepsilon)}\frac{\partial E(\varepsilon)}{\partial \varepsilon}$,[19] where $V(\varepsilon)$ is the volume at strain ε. The ideal strength of crystal refers to the first maximum or minimum point of the stress–strain curve reached during the tensile or compressive deformation, respectively. The corresponding stress and strain at this point are presented as the first maximum (minimum) stress (σ_{FM}) and the first maximum (minimum) strain ($\varepsilon_{\mathrm{FM}}$), respectively.[6] The lines in Figs. 2(b), 2(d), and 2(f) formed by the red triangles represent the first derivatives of the stress–strain curve, $\frac{\mathrm{d}}{\mathrm{d}\varepsilon}[\frac{1}{V(\varepsilon)}\frac{\partial E(\varepsilon)}{\partial \varepsilon}]$, which could measure the sensitivity to change of the stress with respect to a change in the strain. The calculation results indicate that the behaviors of the stress–strain curves of TiB_2 differ little at small strains $(-0.1, -0.1)$ along any of the three primary directions. Monotonically increasing proportionality up to almost 25% the total strain domain can be found and indicates that the present deformation is an elastic deformation. However, the anisotropy of the stress–strain relation of TiB_2 begins to manifest at larger strains, both in tension and in compression.

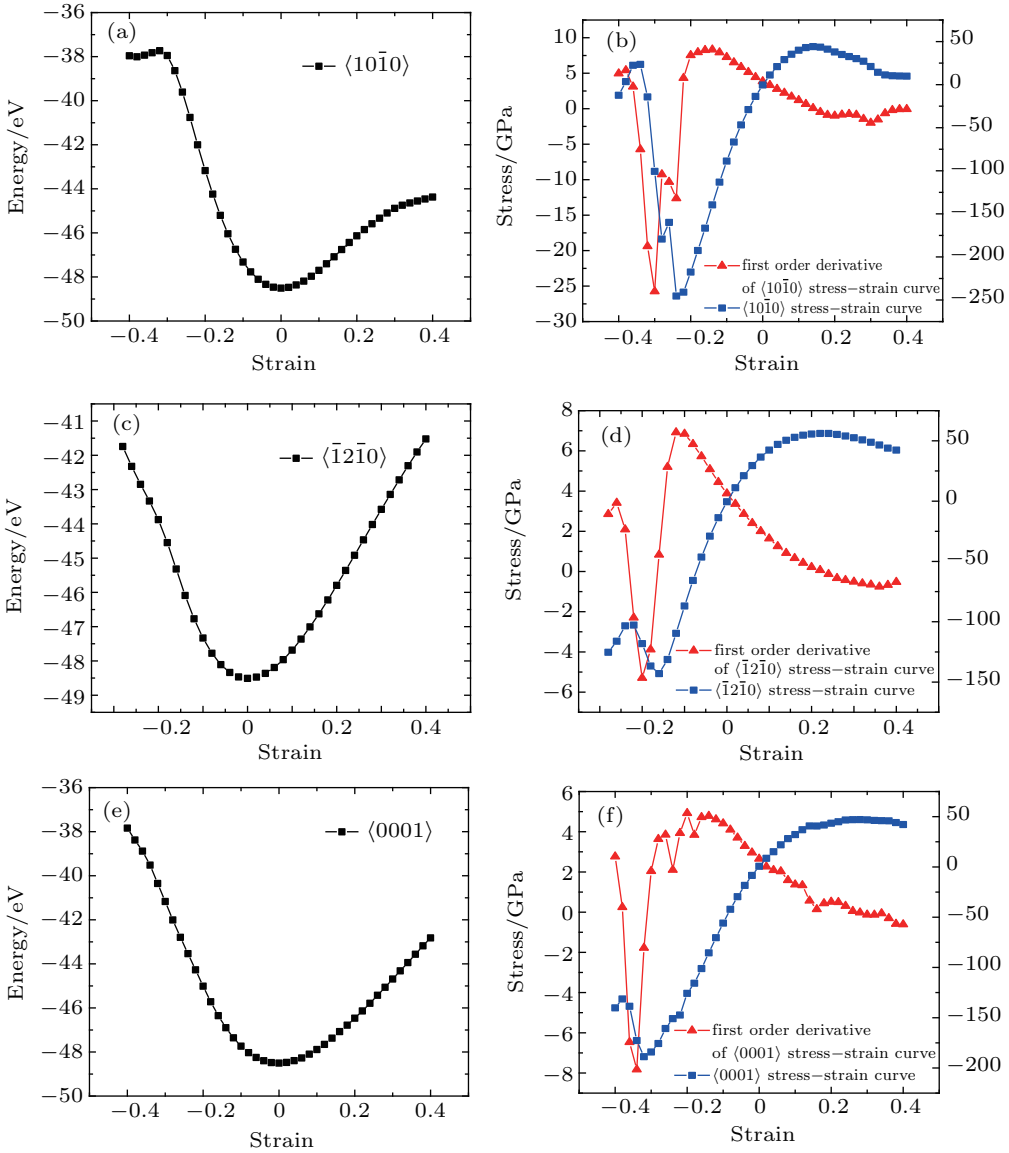


Fig. 2. (a), (c), (e) Energy and (b), (d), (f) stress as a function of deformed strain for TiB_2 under uniaxial tension and compression along the $\langle 10\bar{1}0\rangle$, $\langle \bar{1}2\bar{1}0\rangle$, and $\langle 0001\rangle$ directions.

The ideal tensile strengths of the three principle directions of TiB_2 show an increasing tendency $\sigma_{\langle 10\bar{1}0\rangle} = 44.13$ GPa $< \sigma_{\langle 0001\rangle} = 47.03$ GPa $< \sigma_{\langle \bar{1}2\bar{1}0\rangle} = 56.09$ GPa, at strains 0.14, 0.28, and 0.22, respectively. The ideal compressive strengths of the three principle directions of TiB_2 show an increasing tendency $|\sigma_{\langle \bar{1}2\bar{1}0\rangle}| = 142.96$ GPa $< |\sigma_{\langle 0001\rangle}| = 188.75$ GPa $< |\sigma_{\langle 10\bar{1}0\rangle}| = 245.33$ GPa, at strains -0.16, -0.32, and -0.24, respectively. The trends for tensile and compressive strengths are just the opposite. Along the $\langle 10\bar{1}0\rangle$ direction, the compressive strength is about 72% lower than that of the strongest $\langle \bar{1}2\bar{1}0\rangle$ direction, while its tensile strength is almost 21% higher than that of the weakest $\langle \bar{1}2\bar{1}0\rangle$ direction. This manifests a strong mechanical anisotropy in the (0001) plane.

From Figs. 2(b), 2(d), and 2(f), it can be seen that the stress–strain curves are noticeably compression–tension anisomerous for all of the three directions. Like most structural ceramics, TiB_2 is considerably stronger under compression than in tension. The asymmetric ratios of the ideal compressive to tensile strengths are 5.56, 2.55, and 4.01 for the crystallographic directions $\langle 10\bar{1}0\rangle$, $\langle \bar{1}2\bar{1}0\rangle$, and $\langle 0001\rangle$, respectively. It can be expected that this compression tension asymmetry also exists in other AlB_2-type transition metal diborides, such as ZrB_2 and HfB_2.

3.4. Electronic structure analysis

Figure 3 gives the total and partial densities of states (TDOS and PDOS) of unstrained TiB_2 and TiB_2 at ε_{FM} 0.14, -0.24 for tension and compression along the direction $\langle 10\bar{1}0\rangle$, 0.22 and -0.16 for tension and compression along the direction $\langle \bar{1}2\bar{1}0\rangle$, and 0.28, -0.32 for tension and compression along the direction $\langle 0001\rangle$, where the vertical line indicates the Fermi level E_F. Three features are obvious in the density of states of TiB_2. First, the peak at low energies (~ -15 to -7 eV) can mainly be attributed to localized B-2s electrons.

Second, around −1 eV to −5 eV, the bonding states of Ti-d and B-2p electrons can be found. It indicates a covalent interaction between them resulting from the strong hybridization. The strong hybridization of the Ti-3d and B-2p can lower the energy of the bonding states and increase that of the anti-bonding states, which produces the pseudogap near the Fermi level.[35,36] The existence of the pseudogap helps effectively resist the elastic and plastic deformations and results in high elastic moduli and ideal strengths.[37,38] Third, above the pseudogap there are antibonding states dominated by Ti.

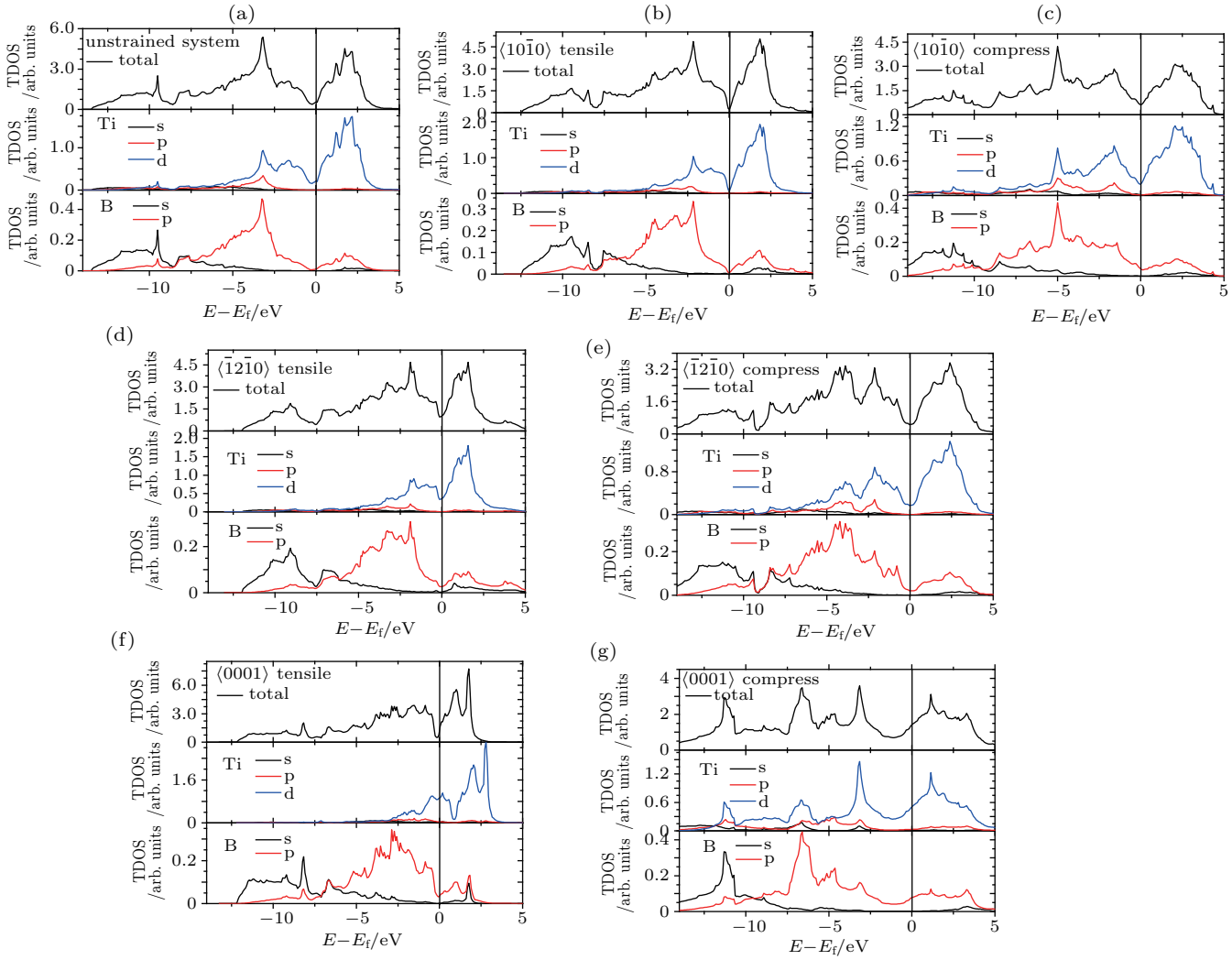


Fig. 3. The total and site projected densities of states (TDOS and PDOS) of TiB_2 at strains (a) 0.00, (b) 0.14, (c) −0.24 along the direction ⟨10$\bar{1}$0⟩, (d) 0.22, (e) −0.16 along the direction ⟨$\bar{1}$2$\bar{1}$0⟩, and (f) 0.28, (g) −0.32 along the direction ⟨0001⟩. The vertical line indicates the Fermi level E_F.

Going from the unstrained system to TiB_2 under tension and compression, the bonding peaks of Ti-3d and B-2p are moved to higher energy. In Figs. 3(g) and 3(f), E_F is no longer located at the bottom of the pseudogap, and is shifted to the region implying occupation of anti-bonding states instead. The above two findings are consistent with the predicted reduced structural stability of TiB_2.

4. Conclusions

We have investigated the anisotropic elastic properties, ideal compressive and tensile strength, and critical strain of TiB_2 by first-principles calculations. The lattice constant c is larger than a due to the anisotropic chemical bonding intra- and inter-the boron layers. The obtained elastic constants could clearly indicate the anisotropic elasticity of the TiB_2 structure. Because the covalent B–B bond is much stronger than the ionic-covalent Ti–B bond. Based on the obtained elastic and compliance constants, the bulk modulus and shear modulus were calculated according to the Voigt–Reuss–Hill method. The Young's modulus, Poisson' ratio, and hardness were also estimated and discussed. Our data fit the other theoretical and experimental results quite well. The inflexion points of the energy–strain curves for [10$\bar{1}$0], [$\bar{1}$2$\bar{1}$0], and [0001] uniaxial loadings occur at $\varepsilon = 0.16, 0.26, 0.36$ for tension and $\varepsilon = -0.22, -0.16, -0.30$ for compression. The ideal compressive and tensile strengths of TiB_2 show opposite changing tendencies for the three primary directions. The ideal tensile strengths vary from $\sigma_{\langle\bar{1}0\bar{1}0\rangle} = 44.13$ GPa, $\sigma_{\langle 0001\rangle} =$

47.03 GPa to $\sigma_{\langle\bar{1}2\bar{1}0\rangle} = 56.09$ GPa, at strains 0.14, 0.28, and 0.22, respectively. While the ideal compressive strengths vary from $|\sigma_{\langle\bar{1}2\bar{1}0\rangle}| = 142.96$ GPa, $|\sigma_{\langle 0001\rangle}| = 188.75$ GPa to $|\sigma_{\langle 10\bar{1}0\rangle}| = 245.33$ GPa, at strains -0.16, -0.32, and -0.24, respectively. The theoretical investigation shows that the stress–strain curves of TiB_2 are compression–tension asymmetric, and TiB_2 is much stronger under compression than in tension. The ratios of the ideal compressive to tensile strengths are 5.56, 2.55, and 4.01 for the directions $\langle 10\bar{1}0\rangle$, $\langle\bar{1}2\bar{1}0\rangle$, and $\langle 0001\rangle$. The existence of the pseudogap in the DOS of TiB_2 is the result of strong hybridization between Ti-3d and B-2p and indicates a covalent interaction between them. As for TiB_2 under tension and compression, the main peaks of Ti-d and B-2p are shifted towards high energy and E_F moves to the region of anti-bonding states, which manifest the reduced structural stability of TiB_2.

References

[1] Cheng T B and Li W G 2015 *J. Am. Ceram. Soc.* **98** 190
[2] Xiang H M, Feng Z H, Li Z P and Zhou Y C 2015 *J. Appl. Phys.* **117** 225902
[3] Sun L, Gao Y M, Xiao B, Li Y F and Wang G L 2013 *J. Alloy Compd.* **579** 457
[4] Pokluda J, Cerný, M, Šob M and Umeno Y 2015 *Prog. Mater. Sci.* **73** 127
[5] Price D L, Cooper B R and Wills J M 1992 *Phys. Rev. B* **46** 11368
[6] Wen M R and W C Y 2018 *Phys. Rev. B* **97** 024101
[7] Luo X G, Liu Z Y and Xu B 2010 *J. Phys. Chem. C* **114** 17851
[8] Zhou Y C, Xiang H M and Feng Z H 2015 *J. Mater. Sci. Technol.* **31** 285
[9] Zhang X H, Luo X G, Li J P, Hu P and Han J C 2010 *Scr. Mater.* **62** 625
[10] Cheng T B and Li W G 2015 *J. Am. Ceram. Soc.* **98** 190
[11] Saai A, Wang Z H, Pezzotta M, Friis J, Ratvik A P and Vullum P E 2018 *TMS Annu. Meeting & Exhibition TMS* 2018*: Light Metals* **2018** 1329
[12] Munro R G 2000 *J. Res. Natl. Stand. Technol.* **105** 709
[13] Zhang Y, Fukuoka K, Kikuchi M, Kodama M, Shibata K and Mashimo T 2006 *J. Appl. Phys.* **100** 113536
[14] Perdew J P, Burke K and Ernzerhof M 1996 *Phys. Rev. Lett.* **77** 3865
[15] Kresse G and Furthmüller J 1996 *Phys. Rev. B* **54** 11169
[16] Monkhorst H J and Pack J D 1976 *Phys. Rev. B* **13** 5188
[17] Milman V and Warren M C 2001 *J. Phys.: Condens. Matter* **13** 241
[18] Reshak A H and Jamal M 2012 *J. Alloy Compd.* **543** 147
[19] Roundy D, Krenn C R, Cohen M L and Morris J W 1999 *Phys. Rev. Lett.* **82** 2713
[20] Zhang Y, Sun H and Chen C F 2004 *Phys. Rev. Lett.* **93** 195504
[21] Waskowska A, Gerward L, Olsen J S, Babu K R, Vaitheeswaran G, Kanchana V, Svane A, Filipov V B, Levchenko G and Lyaschenko A 2011 *Acta Mater.* **59** 4886
[22] Spoor P S, Maynard J D, Pan M J, Green D J, Hellmann J R and Tanaka T 1997 *Appl. Phys. Lett.* **70** 1959
[23] Mizuno M, Tanaka I and Adachi H 1999 *Phys. Rev. B* **59** 15033
[24] Born M and Huang K 1954 *Theory of Crystal Lattices* (London: Oxford University Press)
[25] Okamoto N L, Kusakari M and Tanaka K 2010 *Acta Mater.* **58** 76
[26] Panda K B and Chandran K S R 2006 *Comput. Mater. Sci.* **35** 134
[27] Chung D H and Buessem W R 1967 *J. Appl. Phys.* 38
[28] Voigt W 1928 Lehrbuch der Kristallophysic, Leipaig
[29] Reuss A and Angew Z 1929 *Math. Mech.* **9** 49
[30] Hill R 1952 *Proc. Phys. Soc. A* **65** 349
[31] Chen X Q, Niu H Y, Li D Z and Li Y Y 1920 *Intermetallics* **11** 1275
[32] Kumar R, Mishra M C, Sharma B K, Sharma V, Lowther J E, Vyas V and Sharma G 2012 *Comput. Mater. Sci.* **61** 150
[33] Zhang X, Luo X, Li J, Hu P and Han J 2010 *Scr. Mater.* **62** 625
[34] Pugh S F 1954 *Philos. Mag.* **45** 823
[35] Xu J H and Freeman A J 1990 *Phys. Rev. B* **41** 12553
[36] Vajeeston P, Ravindran P, Ravi C and Asokamani R 2001 *Phys. Rev. B* **63** 045115
[37] Wang Y J and Wang C Y 2009 *Appl. Phys. Lett.* **94** 261909
[38] Martin D, Ulf J and Johanna R 2015 *J. Phys.: Condens. Matter* **27** 435702